SM Online
Scientific Resources
SM Journal of Biology

Review Article

Turbulent Mixing in 2-D and 3-D Density Currents over a Slope

Manjura Nayamatullah and Kiran Bhaganagar*

Department of Civil Engineering, University of Texas, USA

Article Information

Received date: Aug 07, 2017
Accepted date: Aug 24, 2017
Published date: Aug 31, 2017

***Corresponding author**

Kiran Bhaganagar, Associate Professor, Department of Mechanical Engineering, 1 UTSA Blvd, San Antonio, TX 78249, USA, Email: Kiran.bhaganagar@utsa.edu

Abstract

Turbulent Mixing in buoyancy-driven stratified flow can be most accurately represented by two non-dimensional parameters: 'entrainment rate (E)' and 'mixing efficiency (μ)'. This study investigates the differences in mixing between 2-D and 3-D dense currents, with a bottom slope up to 100 for a wide range of Reynolds ($1500 < Re < 17000$) by employing high-resolution Large Eddy Simulations (LES). For given initial conditions, the instantaneous Froude's number for 2-D simulation is equivalent to that from 3-D simulation in the slumping phase. However, the E in the former is up to twice as large as that in the latter, which ranges from $0.02 < E < 0.1$. The results demonstrate strong correlations of E and μ with Re, within the wide span of Re cases, for subcritical Fr within 0.50-.65. It is further shown that μ values are in the range of 0.11 ± 0.02 for 3-D and 0.14 ± 0.01 for 2-D lock-exchange cases, which is smaller than the value of 0.2 that is extensively used by the oceanography community to compute mixing in the ocean. Differences in mixing behavior exist between lock-exchange and dense overflow density current systems.

Introduction

Mixing within density currents plays a fundamental role in predicting and understanding the dynamics of dense current propagation, which are often encountered in the natural environment and numerous fields of science and engineering, including geosciences, geophysics, hydraulics, limnology, oceanography, snow mechanics, and weather prediction [1]. Turbulent mixing of dense and ambient fluids is also a key process for both coastal and deep ocean circulation. The mechanism and dynamics of entrainment or mixing in overflows that are generated at high altitudes, and descend through the continental slope to ocean basins, have been extensively investigated, as a result of their global importance in thermo haline circulation [2-9].

For example, Baines and Condie [10] reported that the down slope transport of dense current on the Antarctic continental slope is largely governed by geostrophy and mixing mechanisms. More recently, Cenedese and Adduce [11] demonstrated that the final properties of the density of North Atlantic deep water, which originated from the Greenland Sea, depend primarily on the entrainment of ambient water in the dense current flowing through the Denmark Strait, Faroe Bank Channel, and continental slope.

For decades, researchers have attempted to gain a better understanding of the physics of mixing in dense current. Prandtl [12] proposed that mixing with the ambient fluid takes place at the head of the dense current. Subsequently, several laboratory experiments have shown that the details of mixing and entrainment in canonical lock-exchange density current systems lead to a considerable increase in the volume of the dense flow [13-21]. Most of the entrainment analysis has been conducted in laboratory tank experiments; whereas very few numerical modeling studies [22-26] have investigated the dynamics of mixing in dense overflow cases. Even with recent advancements in computational methods and computing power, fully-resolved 3-D turbulent density current simulations are prohibitively expensive. In this study, highly resolved 2-D and 3-D large eddy simulations are employed to evaluate the mixing, both quantitatively and qualitatively, in density current systems. The differences between 2-D and 3-D, in terms of flow properties such as front height, front velocity, and Froude number (Fr), have been well studied [27]. However, the differences between entrainment in 2-D and 3-D simulations in mixing analyses of density current is still not clear. Since the primary mechanisms of entrainment of ambient fluid into dense current are Kelvin-Helmholtz instabilities that are 2-D in nature, it is well worth looking into the mixing differences between 2-D and 3-D simulations; indeed, this is the primary objective of this study. In the process of assessing the mixing behavior in both kinds of simulation, a robust and accurate method for quantifying the entrainment rate is employed; this is capable of incorporating all the mixed fluid that is generated at the shear interface of dense current. A wide range of Reynolds number ($1500 < Re < 17000$) cases within subcritical conditions, $0.5 < Fr < 0.65$, are simulated within the scope of this study. To our knowledge, this is one of the first numerical studies to investigate mixing in lock-exchange and dense overflows using 2-D and 3-D LES simulations within the extreme range of Re.

In a similar way to the entrainment rate, turbulent mixing in two distinct water masses can be presented as mixing efficiency (μ), which has been extensively used within the oceanography community. Such efficiency in stratified flow is of vast importance in deep ocean modeling, and therefore a substantial amount of experimental and numerical studies have been carried out to quantify an appropriate mixing efficiency value; this last is still being debated. Most ocean circulation models assume this value, in turbulent flows, to be constant at 0.2; however, the results of several numerical and experimental studies are in conflict with this finding.

Arneberg [5] provided two different efficiency metrics for mixing in a patchy stratified system. The first, the small-scale mixing efficiency, is defined by the increase of initial potential energy due to small-scale turbulent mixing within the patches. In most laboratory and numerical experiments, the value for this parameter is found to be 0.17~0.2, which provides an insight into turbulent mixing efficiencies. The second, the large-scale mixing efficiency, is obtained after the mixed fluid has collapsed laterally in the system. This is a relevant parameter for determining large-scale irreversible changes in the stratification caused by mixing; its value is generally found to be 0.11. Arneberg [5] also showed that the large-scale mixing efficiency is always smaller than its small-scale counterpart by a factor of 2. Prastowo et al. [28] estimated the mixing efficiency in hydraulically controlled buoyancy-driven exchange flows through a constriction, and estimated the μ, attaining a value of 0.11 (± 0.01). Later, Ilicak [29] studied the energetics and mixing efficiency of 3-D lock-exchange flow, showing that the μ in the latter is smaller than 0.2 and saturates around 0.12 for Re > 2500. Peltier and Caulfield [30] studied the mixing efficiency in stratified shear flows, providing an explanation of the numerical value of μ as 0.2, which has been observed in a range of experimental studies. These authors proposed that the efficiency of the mixing, which occurs immediately after the initially two-dimensional nonlinear Kelvin-Helmholtz instability matures, is rather high, typically of the order of 70%; however, this eventually decreases with time to reach a value of 0.15. In our study, the method proposed by Prastowo et al. [28] is adopted to evaluate the mixing efficiency of 2-D and 3-D lock-exchange cases within the scope of our research.

The primary aim of this study is to attain an insight into the differences between mixing in 2-D and 3-D LES simulations, employing dense overflows and lock-exchange cases. We investigate the mixing dependency using the efficiency and entrainment parameters as metrics. For this purpose, LES is used as a tool to simulate lock-exchange and constant flux within the extreme range of Re cases. The paper is organized as follows: the details of problem formulation and the numerical approach are presented in Section 2. Details of the entrainment quantification are given in Section 3, the mixing efficiency quantification is covered in Section 4, and the results are discussed in Section 5. Section 6 offers conclusions.

Problem formulation and the numerical approach

In a lock-exchange system, two liquids with densities of ρ1 (heavy) and ρ2 (light or ambient) were placed into an inclined channel of height H, length L, and angle of inclination θ; these were initially separated by a lock located at a distance of L1 from the left-side wall. Upon removal of the lock gate at time t = 0, due to the sudden release of the fixed volume of the heavy fluid into its ambient counterpart, the former slumped to the bottom. This resulted in the formation of dense currents, which moved horizontally. As the current advanced forward, it entrained the ambient fluid into it. Overflows were well approximated as constant flux systems, wherein the dense fluid entered the channel that was filled with ambient fluid at a constant flux q [m^2/s]. The top of the channel was assumed to be a free surface (slip boundary) and the bottom to be a wall (no-slip boundary).

The details of the numerical algorithm, temporal and spatial schemes, initial and boundary conditions and validation of the solver are presented below: The LES solver is used to solve 3-D incompressible Navier-Stokes equations using the Boussinesq approximation. Transport equations for momentum and scalar density are solved in finite-volume formulation. A conservative form of the Navier-Stokes equation is solved on non-uniform Cartesian meshes. Considering Boussinesq approximation, the constant-density filtered Navier-Stokes equations and the advection-diffusion equation for the density ρ are solved. The filtered governing equations are:

Continuity Equation:

$$\frac{\partial \overline{u_i}}{\partial x_i} = 0 \tag{1}$$

Where, u_i is filtered velocity to be used in LES.

Momentum Equation:

The momentum equation for the filtered velocity field can be written as:

$$\frac{\partial \overline{u_i}}{\partial t} + \frac{\partial (\overline{u_i u_j})}{\partial x_j} = -\frac{1}{\rho_0}\frac{\partial \overline{p}}{\partial x_i} + \frac{1}{\rho_0}\frac{\partial (\tau_{ij} + \tau_{tij})}{\partial x_j} + \frac{\overline{\rho}}{\rho_0} g_i \tag{2}$$

Where, τ_{ij} is the shear stress due to viscous effect caused by turbulent eddies and:

$$\tau_{ij} = \mu\left[\left(\frac{\partial \overline{u_i}}{\partial x_j} + \frac{\partial \overline{u_j}}{\partial x_i}\right) - \frac{2}{3}\left(\frac{\partial \overline{u_k}}{\partial x_k}\right)\delta_{ij}\right] \tag{3}$$

where μ is the molecular dynamic viscosity. Substituting the expression for τ_0 in equation 2, assuming constant molecular viscosity $\mu = \mu_0$ we get:

$$\frac{\partial \overline{u_i}}{\partial t} + \frac{\partial (\overline{u_i u_j})}{\partial x_j} = -\frac{1}{\rho_0}\frac{\partial \overline{p}}{\partial x_i} + \nu_0 \frac{\partial}{\partial x_j}\left[\left(\frac{\partial \overline{u_i}}{\partial x_j} + \frac{\partial \overline{u_j}}{\partial x_i}\right) - \frac{2}{3}\left(\frac{\partial \overline{u_k}}{\partial x_k}\right)\delta_{ij}\right] - \frac{\partial R_{ij}}{\partial x_j} + \frac{\overline{\rho}}{\rho_0} g_i \tag{4}$$

where $\mu = \mu_0$ and R_{ij} is SGS stress tensor that replaces τ_{tij}. Applying continuity constraint for incompressible flow we get:

$$\frac{\partial \overline{u_i}}{\partial t} + \frac{\partial (\overline{u_i u_j})}{\partial x_j} = -\frac{1}{\rho_0}\frac{\partial \overline{p}}{\partial x_i} + \nu_0 \frac{\partial}{\partial x_j}\left(\frac{\partial \overline{u_i}}{\partial x_j}\right) - \frac{\partial R_{ij}}{\partial x_j} + \frac{\overline{\rho}}{\rho_0} g_i \tag{5}$$

Substituting Equation 1 in Equation 5 we get:

$$\frac{\partial \overline{u_i}}{\partial t} + \frac{\partial (\overline{u_i u_j})}{\partial x_j} = -\frac{1}{\rho_0}\frac{\partial \overline{p}}{\partial x_i} + \nu_0 \frac{\partial}{\partial x_j}\left(\frac{\partial \overline{u_i}}{\partial x_j}\right) + \nu_t \frac{\partial}{\partial x_j}\left(\frac{\partial \overline{u_i}}{\partial x_j}\right) - \frac{2}{3} k\delta_{ij} + \frac{\overline{\rho}}{\rho_0} g_i \tag{6}$$

$$\frac{\partial \overline{u_i}}{\partial t}+\frac{\partial(\overline{u_i u_j})}{\partial x_j}=-\frac{\partial}{\partial x_i}\left(\frac{\overline{p}}{\rho_0}+\frac{2}{3}k\right)+(\nu_0+\nu_t)\frac{\partial}{\partial x_j}\left(\frac{\partial \overline{u_i}}{\partial x_j}\right)+\frac{\overline{\rho}}{\rho_0}g_i \quad (7)$$

The additional term within the parenthesis of pressure gradient in-effect leads to the calculation of modified or resolved kinematic pressure. Nevertheless, the contribution of the isotropic part of Reynolds stresses is negligible with respect to the static pressure field. Thus the additional term clubbed to the pressure field projects negligible influence. Boussinesq approximation is realized in the last term of Equation 7 where density variations are assumed to contribute only in the gravity term. Henceforth the sum ($\nu_{tt} + \nu_0$) is denoted as ν_{eff}. The scalar transport equation is solved, where in the variation in density field is evaluated with the help of an additional scalar transport equation:

$$\frac{\partial \overline{\rho}}{\partial t}+\frac{\partial(\overline{\rho u_j})}{\partial x_j}=\frac{\partial}{\partial x_j}\left(K_{eff}\frac{\partial \overline{\rho}}{\partial x_j}\right) \quad (8)$$

Where $K_{eff}=\frac{\nu_t}{Sc_t}+\frac{\nu_0}{Sc}$

Dynamic Smagorinsky eddy viscosity model is used to solve the turbulence equations. It gives more robust and accurate estimation of turbulence and eddies as the Smagorinsky constant (Cs) is recalculated dynamically in every iteration as a function of space and time to follow the changes in the fluid. Besides, in near wall region the dynamic Smagorinsky model is able to damp the Smagorinsky coefficient due to use of the dynamic procedure, which relaxed the need for additional damping function (i.e. Van Driest damping like in constant Smagorinsky model). Özgökmen et al. also showed that the dynamic Smagorinsky model lead in significant improvement of accuracy in the prediction of mixing compared to constant-coefficient Smagorinsky model in lock-exchange density current problem.

All equations are discretized with a second-order bounded implicit central-difference Crank-Nicholson scheme. The convective terms have been discretized using a second-order bounded central-difference scheme. A Gauss scheme with linear interpolation was used to discretize the diffusive terms in the momentum equation. At the bottom (wall), a no-slip boundary condition is applied for the velocity and zero flux conditions of the density field. A zero normal gradient for velocity and density fields is employed at the top free surface, at the inlet, and at the outlet boundary. The flow is assumed to be periodic in the spanwise direction. The flow field is initialized with zero velocity throughout the domain, and a random disturbance (1%) was applied to the density field to trigger turbulence. The serial code has been parallelized using MPI based on the domain decomposition technique. The time step (d_t) was estimated amidst the simulation run to maintain the courant number within the range of 0.35~0.5 with excellent accuracy of capturing mixing physics by optimum computational cost. The Gauss scheme with linear interpolation had been employed for diffusive terms (Laplacian) in momentum equation. The simulations were performed with grid spacing of 10-3, and mesh of size 700x125x100. Grid convergence has been obtained at this mesh resolution.

The height of channel H was adopted as the length scale, while the buoyancy velocity

$U_b=\sqrt{g'H\cos\theta}$ was chosen as the velocity scale; consequently, the time scale was taken as

$t_0=\frac{H}{U_b}$ dimensionless density, which ranged from 0 to 1, and reduced gravity g_0:

$$\overline{\rho}=\frac{\rho-\rho_2}{\rho_1-\rho_2} \text{ and } g'=g\left(\frac{\rho_1-\rho_2}{\rho_2}\right)$$

The dimensionless parameters' Reynolds Number (Re) was based on front velocity (Uf) and front height (hf), while another dimensionless parameter for the Froude Number (Fr) was defined as:

$$\mathrm{Re}=\frac{U_f h_f}{\vartheta} \text{ and } Fr=\frac{U_f}{\sqrt{g'H\cos\theta}}$$

The front height is defined as the maximum height of the current at 10% threshold value. Validation of 3-D LES solver of lock-exchange currents over horizontal surface has been performed by comparing the front conditions with well-established Direct Numerical Simulation (DNS) solver of Bhaganagar (2014). A comparison of front location xf for the density currents with time closely matched with DNS results. Further, at the Reynolds number of 4000, Froude number has been estimated as 0.59 using equation in our case, which is close match with DNS 8 studies of Bhaganagar (2012) and Hartel et al. [31] where they obtained Fr for smooth wall as 0.6 and 0.61 respectively. In addition to the front conditions, instantaneous 2-D and 3-D density and velocity structures demonstrated a good match with DNS results. The details of numerical simulation for lock-exchange release currents and for constant flux overflows is shown in Table 1.

Details of Entrainment Quantification Methodology

Traditionally, entrainment has been calculated from the first principle, using a variety of approaches. Morton et al. [32] assumed that the velocity at which ambient fluid enters the density current (w_E) are linearly proportional to the mean downstream velocity U, which is often expressed in terms of an entrainment ratio that is defined as $E=\frac{w_E}{U}$. Ellison and Turner and Britter and Linden expanded on this concept, while for bottom gravity currents, [14] approximated the entrainment rate as the rate of change of the current's thickness, with stream-wise distance as $E=\frac{dh}{dx}$. However, at different times, the estimation of W_E or E is highly difficult, due to the presence of turbulence and instabilities in the shear interface. Therefore, in this study, we employed the "volume increment" method, which can estimate entrainment; this technique is similar in concept to previous definitions by Meleshko. In this section, we demonstrate the various approaches to estimating the volume of mixed fluid, before laying out the entrainment parameter in appropriate detail, which has not been observed in previous studies on stratified shear flow.

Volume increment method

We evaluate the net entrainment parameter as the entrainment per length of the current (E_l). For this purpose, the net entrainment parameter is defined as increase in the volume of fluid in the current from the initial lock volume scaled by a length scale, length of the

Table 1: 2-D and 3-D lock exchange release (L-E) and constant flux overflows (C-F) simulations have been performed in domain of size 2.4mx0.2mx0.25m. The initial reduced gravity (g_o), slope of the bottom surface, buoyancy velocity (μ_b), averaged front velocity during slumping phase (μmf), averaged height of the current (hmf) are varied. Local- Reynolds number (Re) and Froude number (Fr) are calculated based on averaged- front velocity and front height during slumping phase.

Case	Slope	g'	U_f	H_f	Re	Fr
3-D L-E	0	0.007	0.016	0.1	1584	0.604743157
3-D L-E	0	0.027	0.032	0.1	3168	0.615840287
3-D L-E	0	0.11	0.064	0.1	6337	0.610216057
3-D L-E	0	0.19	0.088	0.1	8713	0.6384191
3-D L-E	5	0.02	0.028	0.1205	3341	0.571448895
3-D L-E	10	0.02	0.0284	0.1225	3445	0.578175345
3-D L-E	20	0.02	0.029	0.1245	3575	0.599522403
3-D L-E	5	0.05	0.0455	0.1268	5712	0.572525263
3-D L-E	10	0.05	0.0465	0.127	5847	0.588017648
3-D L-E	20	0.05	0.0477	0.1275	6022	0.616290362
3-D L-E	5	0.1	0.063	0.1295	8078	0.554668563
3-D L-E	10	0.1	0.0665	0.1325	8724	0.582154122
3-D L-E	20	0.1	0.0681	0.1365	9204	0.601295395
3-D L-E	5	0.45	0.13	0.107	13772	0.594
3-D C-F	10	0.45	0.127	0.135	16975	0.519
3-D C-F	20	0.45	0.121	0.15	17970	0.480
3-D C-F	0	0.45	0.127	0.095	11946	0.614
3-D C-F	0	0.45	0.098	0.057	5531	0.612
3-D C-F	0	0.45	0.088	0.04	3485	0.656
2-D L-E	0	0.05	0.044	0.1	4356	0.622
2-D L-E	5	0.05	0.0455	0.1175	5293	0.595
2-D L-E	10	0.05	0.0465	0.1215	5594	0.601
2-D L-E	20	0.05	0.0475	0.1285	6043	0.611
2-D C-F	5	0.45	0.13	0.107	13772	0.594
2-D C-F	10	0.45	0.127	0.135	16975	0.519
2-D C-F	20	0.45	0.121	0.15	17970	0.480
2-D C-F	0	0.45	0.127	0.095	11946	0.614
2-D C-F	0	0.45	0.098	0.07	6792	0.552
2-D C-F	0	0.45	0.088	0.053	4618	0.570
2-D L-E	0	0.007	0.0157	0.1	1554	0.593
2-D L-E	0	0.027	0.029	0.1	2871	0.558
2-D L-E	0	0.11	0.0635	0.1	6287	0.605
2-D L-E	0	0.19	0.087	0.1	8614	0.631

density current ($l=X_b-X_f$), and a velocity scale, front velocity, to calculate entrainment at every time step. This is a representation of the total increase in the volume of the mixed fluid in the current at that instant of time with respect to the lock-volume. The volume change in the system represents the amount of ambient fluid that is entrained into the current. The length of the current (l) is calculated between the nose and tail of the current for a lock-exchange system (Figure 1), and for constant flux cases, it is estimated as the distance of the nose from a reference point (x_0). The velocity scale (v) is the front velocity (U_f) of the current. It is important to note that the volume 'V' referred to in this study indicates the volume per unit width, essentially representing the area of current.

$$E = \frac{V(t) - V_0(t)}{t \times \bar{l}(t) \times \bar{v}(t)} \quad (9)$$

As mentioned earlier, the most challenging aspect of calculating E using the volume increment method is the estimation of the current's volume at a given time t. Interface identification approach is used in estimating this volume.

Interface identification: In this technique, the first step is to identify the interface of mixed and ambient fluids to obtain the current height profile (h (x, t)), employing the density threshold scheme for a specific

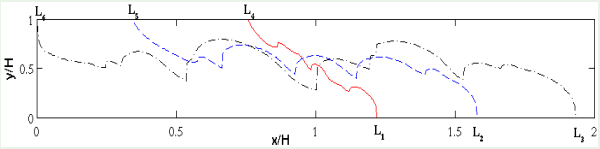

Figure 1: At different times, from the above densities, the current height profile's length scale would be denoted by the red line (L1-L4), blue line (L2-L5), and black line (L3-L6).

value (ρ_c) [33]. Then, the volume of mixed fluid is estimated by integrating the current height profile in a stream-wise direction from the leading edge to the tail of the current. In Figure 2, the green line represents the interface of the mixed and ambient fluids at a specified density threshold value, and the solid black line denotes the interface of the original dense fluid and mixed fluid in the dense current.

$$\rho(x,y,t) = \begin{Bmatrix} 0\, when\, \rho(x,y,t) < \rho_C \\ 1\, when\, \rho(x,y,t) > \rho_C \end{Bmatrix} \quad (10)$$

After evaluating the interfaces or density height profile, as shown in Figure 2, at an instantaneous time (t), the volume of mixed and original dense fluid $V_{(t)}$ and the volume of original dense fluid alone $V_0(t)$ is estimated by integrating the density height profiles from the tail to the nose of the current, as expressed as:

$$V(t) = \int_{X_b}^{X_f} \overline{h(x,t)}\, dx \quad (11)$$

$$V_0(t) = \int_{X_b}^{X_f} \overline{h_0(x,t)}\, dx \quad (12)$$

where h is the height of the mixed fluid, h_0 is the height of the initial dense fluid, and Xf, Xb are the position of the nose, tail of the current, and lock location respectively.

The current height profile is evaluated by tagging the density field where it equals the density threshold value (ρ_c). Depending on the latter, different profiles can be obtained, and the volume of the mixed fluid is estimated from equations (11) and (12). An analysis is performed by varying the density threshold values from 2%-20% to predict the current profile that would provide a tangible and accurate volume estimation for the entrainment parameter. Figure 3 shows the current height profiles for different density threshold value for the

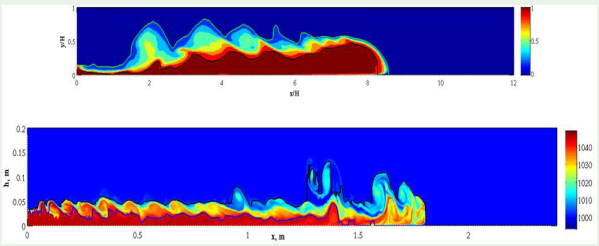

Figure 2: Visual representation of mixed and dense fluid (span-wise averaged density) in a lock exchange case (above) and constant flux case (below).

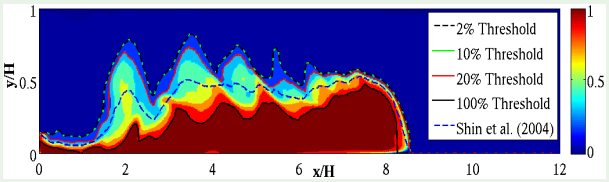

Figure 3: Overlaying current height profiles on a density contour, using Shin et al.'s (2004) method and the threshold technique, for different threshold values.

current during the slumping phase; it is observed that the 2% and 10% thresholds capture almost all the mixed volume in the current, whereas the 20% level excludes a significant portion of the mixed fluid, leading to an under-prediction of the entrainment rate. Figure 3 also clearly shows that the threshold method captures the height profile, to a high degree of precision, for a mixed current; and it predicts better than the Shin [33] method.

In this study, a series of experiments were conducted by varying the density threshold from 2-20%, where the overhanging nose propagated a lock length of 9-10. A thorough and quantitative comparison of both approaches is presented in order to evaluate the entrainment parameter with a bottom slope varying from 00 to 200.

A wide range of density threshold values has been used in various experimental and numerical studies for evaluation of the entrainment. Hacker et al. used six such values, ranging from 5% to 10% of initial density to define the boundary between the mixed and ambient fluids. Özgökmen et al. [34] considered a threshold value of 20% of the ambient density to estimate entrainment in their numerical studies. To assess mixing in particle-driven gravity currents.

Necker et al. [35] varied their threshold from 0 to 12% and showed that the volume of mixed fluid remained constant for a 12% value, but increased significantly for lower values. For lock-exchange gravity currents with a high volume of release, Tokyay et al. [36] evaluated mixing by varying the density threshold from 2% to 20%, finally estimating the mixed volume using a $0.02 < \rho_c < 0.98$ limit. A density threshold value of 10% was used by Hogg et al. [37] in their experimental studies to assess the entrainment in inclined-gravity current-filling basins. Meanwhile, Sher and Woods (2015) used 4% of the initial concentration as a threshold value to identify the height profile, and consequently measured the mixed volume by employing the latter.

In our study, in light of the lack of consistency in threshold criteria, the density threshold value was varied to explore how they could calculate the entrainment parameter and influence the mixing in both lock-exchange and constant flux density current flows. An

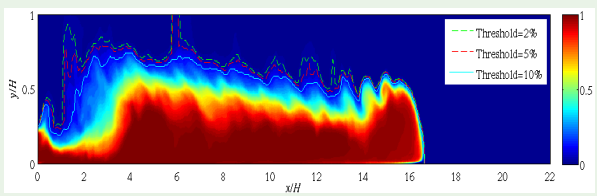

Figure 4: Spanwise averaged density contour overlapped by 2%, 5%, and 10% threshold interfaces for 3-D lock-exchange release currents over horizontal surface at Re=6000.

overlay of 2-D density contour plot with the 2, 5, and 10% threshold lines at t/t_0 = 10 is shown in Figure 4 for a horizontal lock-exchange case with a 0.33 lock-aspect ratio (h/l) and Re = 6000. The analysis revealed that for such cases, the 2% and 5% threshold interfaces included the backflow and over-predicted the volume estimation (Figure 4). However, in qualitative terms, the interface with the 10% threshold captured all the mixed values with greater accuracy.

Further analysis of the threshold's influence on entrainment was carried out by considering two cases of lock-exchange and constant flux density current flows over horizontal bottom surface, within a similar range of Re = 6000. The volume of mixed fluid (VM) was estimated using four threshold values of 2%, 5%, 10%, and 20%. The volume of the mixed fluid increased by a factor of three to four times the initial lock volume over the first eight to ten lock lengths, which is consistent with the findings of Hallworth et al., Marino et al., Sher and Woods and Ottolenghi et al. [18,20,38-40]. Figures 5a show the variations of VM (scaled with initial lock volume) as plotted against the lock number for lock-exchange release currents, and plotted against front location for constant flux currents is shown in Figure 6a. In the lock-exchange case, the mixed volume showed less variance (5-15%) with different ρc for up to five or six lock length distances from the front of the lock gate during the slumping phase. The E calculated using Eq. 9 for lock-exchange release- and constant flux currents are shown in Figure 5b and Figure 6b respectively. For L-E release currents, the E is high at the beginning during the formation of the head or front of the currents and it decreases gradually until the end of the slumping phase, where it reaches a nearly steady value. It is important to note, E is sensitive to the threshold value during the beginning of the slumping phase, whereas for threshold values of 2%-10%, the steady state value of E shows variance of only 2%-7%. On the other hand, constant flux release currents revealed more sensitivity to the threshold values (Figure 6a and 6b).

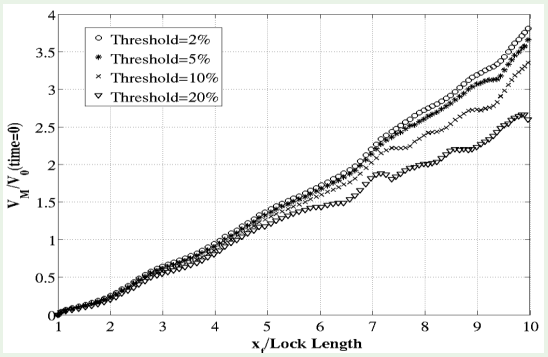

(a)

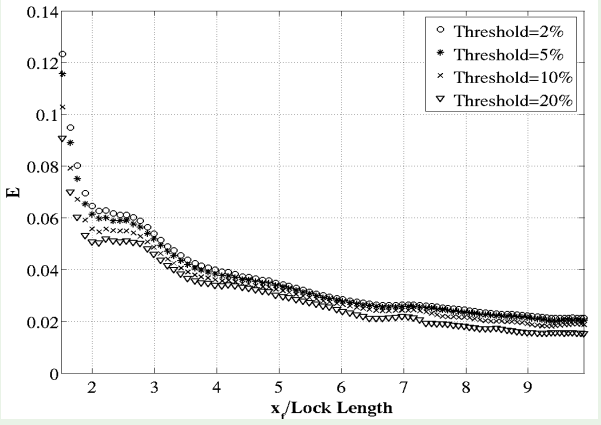

(b)

Figure 5: Threshold effect on the 3-D lock-exchange release currents: (a) *VM /V0*, (b) *E* vs front location scaled by the lock length.

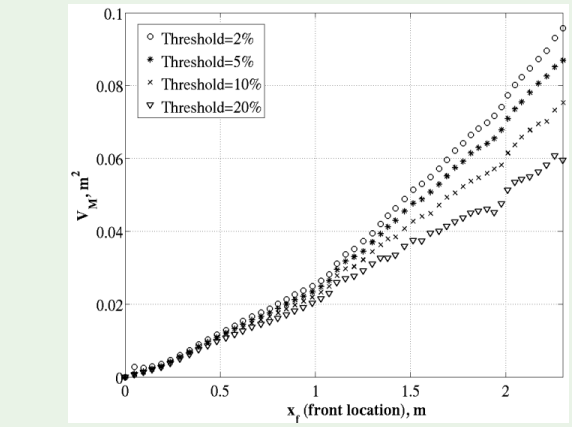

(a)

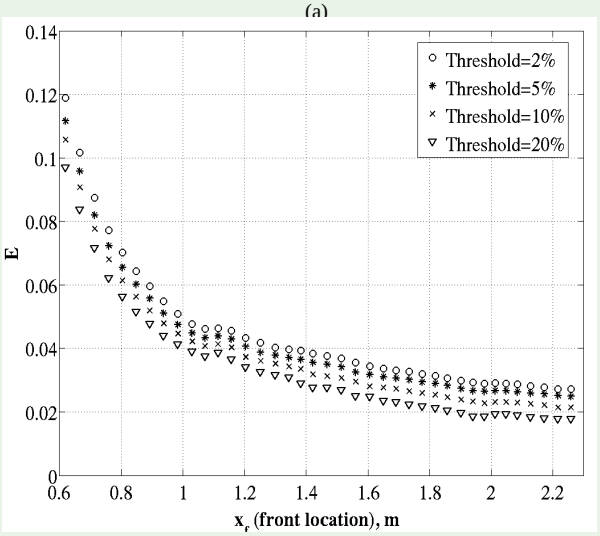

(b)

Figure 6: Threshold effect on the 3-D constant flux release currents: (a) *VM /V0*, (b) *E* vs. front Location.

Next, for lock-exchange flows over slopes of 2.860, 50, and 100, the volumes of mixed fluid and entrainment were measured using 10% density threshold values. Figure 7 shows the spanwise averaged

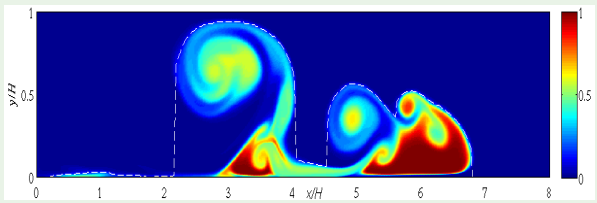

Figure 7: Spanwise averaged density contour overlapped by 10% threshold interface for 3-D lock-exchange release currents over 100 inclined bottom surface.

density contours for 3-D L-E release currents over 100 inclined surfaces. Intense Kelvin-Helmholtz instabilities behind the head are evident for L-E currents released over sloping surfaces. It is important the threshold selected captures the K-H accurately for accurate estimation of mixed volume, and hence the entrainment. The volume calculated using 10% threshold method is shown in Figure 8a as a function of the distance travelled by the front. By applying the threshold approach, Figure 8a shows that the volume of mixed fluid remains similar for up to four lock lengths for all the inclined cases, while from four to seven lock length distances, the VM consistently increased with higher slopes, while for 100-inclined cases, some drastic increases (up to 100%) in the VM were seen beyond seven lock lengths. This rapid increase of mixed volume for 100 sloping cases was observed as a result of the intense Kelvin-Helmholtz instabilities behind the head, which arise due to higher slopes at a later time (Figure 7). It should be noted that for higher-sloping cases, the threshold approach overestimated the mixed volume beyond eight lock lengths. Considering the results discussed above, we will use the 10% density threshold value to evaluate the entrainment in future results and discussion.

Details of Mixing Efficiency Methodology

In addition to the entrainment coefficient, Mixing Efficiency (ME) is another parameter that interprets the mixing in stratified flows such as density currents; it is mostly used by the oceanic community to define the time dependence of volume-averaged energy terms.

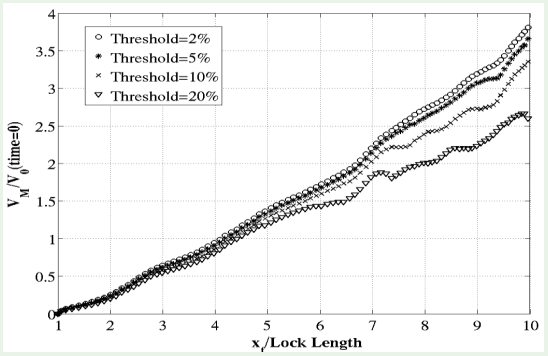

(a)

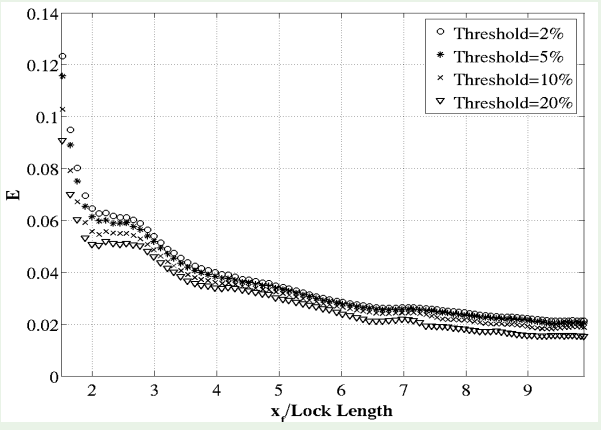

(b)

Figure 8: Effect of the Slope for 3-D lock-exchange release currents: (a) *VM /V0*, (b) *E* vs lock Number.

Mixing removes the available energy from the fluid flow. ME, measure of mixing is defined as the ratio of the irreversible increases in the potential energy to the loss of kinetic energy. Traditionally, the overall efficiency of a flow in converting kinetic energy into potential energy has been defined in terms of a flux Richardson number which is the ratio of spatially and time averaged turbulent buoyancy flux to the sum of averaged turbulent buoyancy flux and turbulent dissipation rate [41]. This ratio can be interpreted as efficiency as the denominator quantifies the total loss rate from the mean kinetic energy reservoir and the numerical quantifies the rate of mixing leading to increase in potential energy. An alternative definition for mixing efficiency is the spatially and time averaged flux coefficient which is the ratio of buoyancy flux to turbulent energy dissipation rate, and for turbulent flows it is assumed approximately constant at 0.2 [6] demonstrated buoyancy flux quantifies the exchange between the potential and kinetic energy reservoirs. However, instantaneous values of buoyancy flux will overestimate mixing, due to time variability, hence requires averaging over sufficiently long scales.

Time dependent separation of mixing from reversible increase of potential energy is obvious from the framework suggested by Winters et al [42] based on the ideas of Lorenz and Thorpe, and which revolve around the concept that the potential energy is partitioned into two parts, the background potential energy and the available potential energy. The maximum potential energy that can be released in this flow is the available potential energy. The background potential energy is the minimum potential energy obtained by sorting the density without mixing. Winters proposed a formalism that is exceedingly straight forward to implement in a numerical simulation.

ME (μ) is the fraction of the total available potential energy released to the flow (which goes into turbulent kinetic energy); this leads to an increase in potential energy through irreversible mixing above the initial background potential energy. ME is given as:

$$\mu = \frac{PE_f - BPE_i}{APE} \tag{13}$$

PEf is the potential energy at the final time, BPEi is the initial background potential energy, and APE is the available potential energy. APE is the difference between initial potential energy and initial background potential energy (the potential energy if there is no mixing).

$$APE = PEi - BPEi \tag{14}$$

One can calculate the initial background potential energy by redistributing the density parcel (ρ^*) with the heaviest at the bottom and lighter parcels above, and then estimating the potential energy for the sorted density parcel throughout the domain, using the following equation:

$$BPE = g\int\int\int \rho^* z dv \tag{15}$$

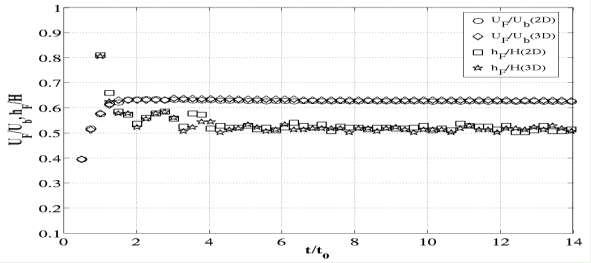

Figure 9: Front velocity and front height in 2-D and 3-D lock-exchange release currents over horizontal surface.

In this study, the method proposed by Prastowo was adopted to evaluate the mixing efficiency in lock-exchange cases within the scope of our study.

Using scaling laws Wells derive a relationship between the entrainment parameter

(E) and flux coefficient (($\overline{\Gamma}$) using bulk Fr as $E = \frac{C}{8}\frac{(\overline{\Gamma})Fr_0^2}{\cos\theta}$ where C is a constant based on averaged depth and length scales of the current. Though a theoretical relation has been established between the flux coefficient and E, due to scarcity of the experimental data, it is not clear as to how does the flux coefficient and E behave at high Re. For subcritical Fr (as in this present study), it was demonstrated that both E and flux coefficient decrease very rapidly with Fr.

Results and Discussion

Comparison of results from 2-D & 3-D simulations

Numerical simulation of 2-D and 3-D lock-exchange release currents and dense overflows with constant flux with similar domain configurations were performed and flow parameters were analyzed was in terms of the flow properties, and mixing quantitative and qualitative methods for Re = 6000.

Flow properties & mixing: Froude's number and front height were estimated for the 2-D and 3-D release dense currents during the slumping phase and plotted against the non-dimensional time, as shown in Figure 9. The Fr and front height for 2-D and 3-D lock-exchange currents are very similar. Ooi et al. [43] also reported similar findings in their lock-exchange numerical studies. However, Ozgokmen et al. [34] numerical study on sloping-bottom density current revealed that the propagation speed in 2-D simulations was

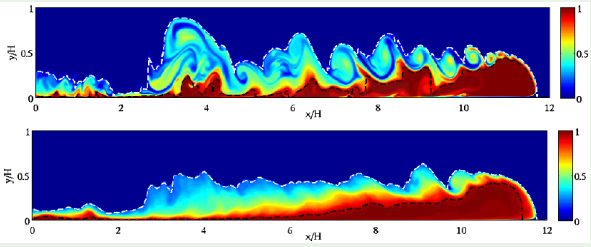

Figure 10: 2-D density contours overlaid by 0.1 density threshold (white dotted line) and original density fluid (black solid line) interface in (top) 2-D simulations; (bottom) 3-D simulations for the horizontal case (bottom slope = 00).

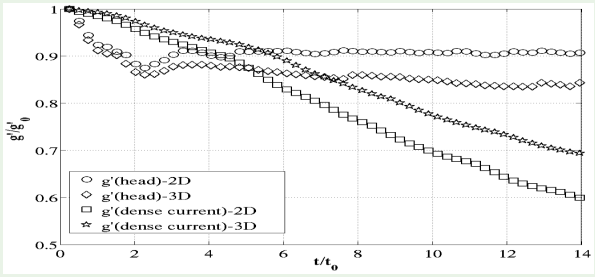

Figure 11: Reduced gravity scaled by initial reduced gravity at head and overall dense current in 2-D and 3-D simulations for bottom slope = 00 lock-exchange case.

approximately 20% slower than that of the 3-D experiments. Next, we compared the qualitative mixing from density contours based on the entrainment rate estimation.

The flow structures of fully developed 2-D and 3-D L-E release density currents over horizontal bottom surface are illustrated as density contour plots in Figure 10 at $t/t_0 = 14$. The span-wise averaged density contour from the 3-D dense currents are compared with the instantaneous density contours of the 2-D currents. It is clear to see that coherent K-H billows break down to small scales behind the head and body region for the 2-D currents, while these instabilities are generated mainly near the head for the 3-D currents. The strong and energetic structures along the shear interface indicate higher mixing for the 2-D currents than the 3-D currents. For the 3-D the lobe-cleft instabilities at the leading edge of the current results in higher dilution in the head region of the current. However, the entrainment of ambient fluid into dense current is more dominant for the 2-D currents. This can be confirmed from Figure 11, wherein the instantaneously reduced gravity (g) in the head region of the front is scaled by initial reduced gravity (g_0); the overall dense current is plotted against the non-dimensional time for both 2-D and 3-D release L-E currents. The reduced gravity value is a good indicator of mixing within the dense current. The average non-dimensional reduced gravity $\left(\overline{g'} = \frac{g'}{g'_0}\right)$ at the current head for the 2-D currents is 0.9, compared to 0.85 for the 3-D currents, which indicates higher mixing in the latter due to 3-D instabilities at the leading edge. However, the lower value of g in the overall dense current in the 2-D currents indicates a higher mixing than in their 3-D counterparts. To gain a comprehensive understanding of the mixing, we compared the entrainment parameters (E) to find that that of the 2-D currents was approximately 50% higher than that of the 3-D currents.

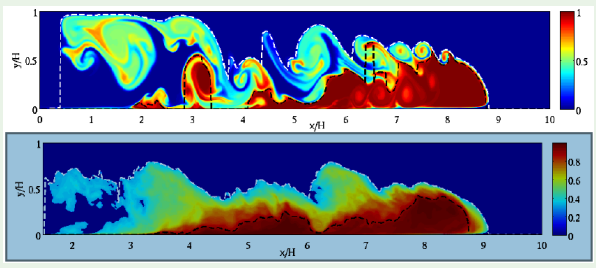

Figure 12: 2-D density contours overlaid by 10% density threshold (white dotted line) and original density fluid (black solid line) interface. (Top): 2-D L-E release currents; (bottom) 3-D L-E release currents over 100 slope.

Citation: Nayamatullah M and Bhaganagar K. Turbulent Mixing in 2-D and 3-D Density Currents over a Slope. SM J Biol. 2017; 3(1): 1016s.

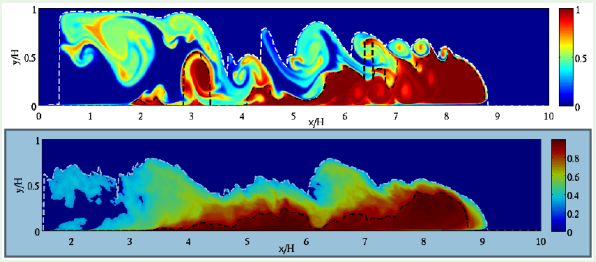

Figure 13: Reduced gravity, scaled by initial reduced gravity, against non-dimensional time at the head and overall dense current in 2-D and 3-D simulations for bottom slope = 100 case.

Next, we investigated the flow structures and mixing for a sloping case of 100 for both 2-D and 3-D dense currents in an accelerating phase. From Figure 12, we observe more energetic K-H rolls in the 2-D currents than in the 3-D currents. Reduced gravity calculated in the head region of the current as well as throughout the entire current is shown in Figure 13. The difference inreduced gravity (g_0) between 2-D and 3-D L-E release currents becomes increasingly significant as the slope steepens, with more mixing in 2-D than in 3-D currents. The entrainment rate (E) of the 2-D L-E release currents is nearly twice as high as of the 3-D L-E currents. Significant differences exist near the head region of the 2-D and 3-D L-E currents. The former undergoes mixing quickly and remains undiluted throughout the accelerating phase, whereas the latter undergoes both mixing and dilution until the end of this phase.

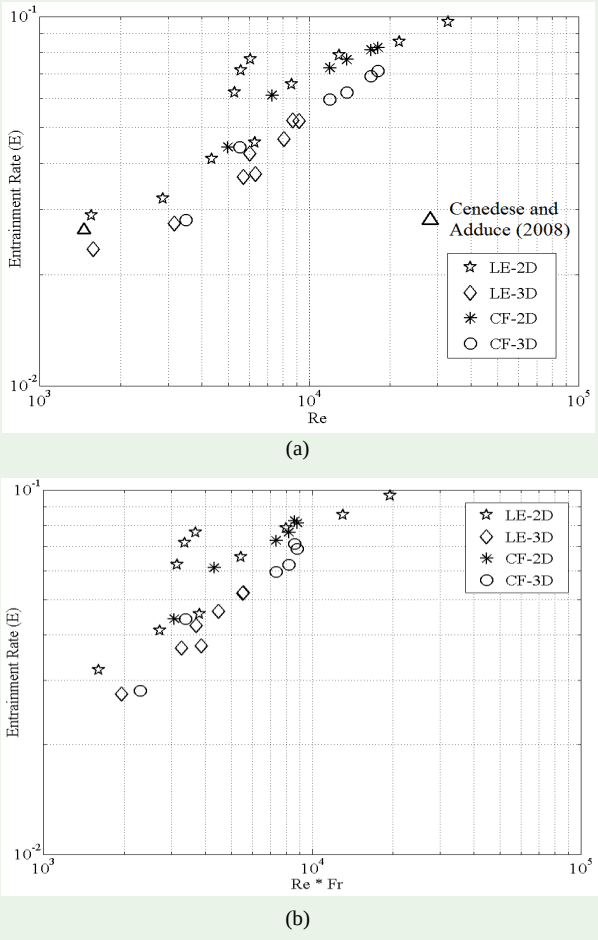

Figure 14: (a) Entrainment parameter versus Reynolds number (*Re*) (b) Entrainment parameter versus production of Reynolds number and Fr.

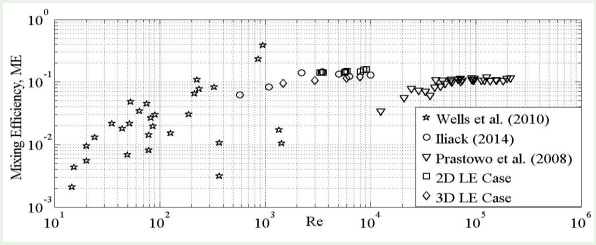

Figure 15: Mixing Efficiency versus Reynolds number (*Re*) for 2-D and 3-D lock-exchanges release currents.

Entrainment dependence on non-dimensional parameter: Figure 14a shows the entrainment parameter calculated using Eq. 9, plotted for a wide range of Re (1500 < Re < 17000), for both 2-D and 3-D lock-exchange currents and constant flux release currents, where Fr remained within subcritical conditions (Fr = 0.5 ≈ 0.65). For 2-D L-E currents, E was higher than in 3-D L-E currents. The entrainment results from our 2-D/3-D LES simulations are in good agreement with Cenedese and Adduce's laboratory-based experimental entrainment results. There is a strong correlation between E and Re. In addition, the rate of increment of E at Re < 104 was higher than that at Re> 104. Cenedese and Adduce conducted a series of dense overflow experiments flowing down a slope in a rotating fluid, and showed a dependency of E on both Re and Fr spanning a wide range of 0.8 < Fr < 10, and 10 < Re < 1400. In Figure 14b, E is plotted versus the product of Re and Fr, which also shows a strong correlation for both 2-D and 3-D lock-exchange currents and dense overflow cases.

Mixing efficiency: Figure 15 shows the mixing efficiency values as plotted against Reynolds number. Also shown in the figures is mixing efficiency using theoretical formulation developed by Wells et al [44] based on experimental data from Cenedese & Adduce. Numerical results from Prestowo and Illiack are also shown. For our cases, the mixing efficiency in the range of 0.14 ± 0.01 for the range of Re considered. The results are smaller than the ongoing, highly debated, and extensively used value of 0.2, as employed by the oceanography community as a mixing efficiency to compute the mixing and energy budget in the ocean. Further, mixing efficiency shows a clear trend with Reynolds number.

Conclusions

Mixing is a profoundly robust and dynamic process, which occurs in most buoyancy-driven stratified flows (such as gravity current or dense overflows), and therefore both alters the final properties of fluid and influences the hydrodynamics of dense currents that propagate downstream. Accordingly, an accurate and computationally efficient method for estimating mixing has enormous significance in both coastal and oceanic circulation. We used a robust LES tool to simulate 2-D and 3-D lock-exchange and dense overflow cases with smooth-sloping bottoms. In addition to the flow properties, the mixing in dense currents, based on entrainment rate and mixing efficiency, were compared between 2-D and 3-D dense lock-exchange and overflows over sloping bottoms for a range of Re (1500 < Re <

32000) cases with subcritical flow conditions (Fr = 0.5 ≈ 0.65). We quantified the E and μ for a series of experimental cases for bottom slopes varying from 00-100. Both 2-D and 3-D currents have the same Fr number during the slumping phase of current evolution in lock-exchange cases. Nonetheless, the entrainment rate (E) values for 2-D currents were up to twice as high as those of the 3-D currents, which ranged from 0.02 < E < 0.1. We observed a strong E dependency on Re within the wide span of Ref cases for both types of simulation. In order to estimate the entrainment rate, the volume increment method was used. E demonstrated sensitivity to the threshold value, and 10% threshold captures significant K-H structures. The mixing efficiency of the 3-D currents were in the range of 0.11 ± 0.02, which is an excellent match with previous numerical and experimental studies; meanwhile, we observed results of 0.14 ± 0.01 for the 2-D currents in the lock-exchange cases, which is approximately 25% higher than the numerical results of Prastowo and comparable to than those of Illiack. However, the results from both types of simulation were smaller than the value of 0.2 that is extensively used by the oceanography community to compute mixing in the ocean. The results demonstrate strong correlations of E and with Re, within the wide span of Re cases, for subcritical Fr within 0.50-.65. It is further shown that μ values are in the range of 0.11 ± 0.02 for 3-D and 0.14 ± 0.01 for 2-D lock-exchange cases. Increasing the Reynolds number increases the buoyancy flux and hence increases the entrainment and mixing efficiency for lock-exchange flows at subcritical Fr is an important conclusion of the present study.

References

1. Simpson, JE. Gravity currents in the environment and the laboratory. Cambridge: Cambridge University Press, 1997.
2. Baines, P. G. Mixing in flows down gentle slopes into stratified environments. Journal Fluid Mechanics, 2001; 443: 237-270.
3. Baines, P. G. Two-dimensional plumes in stratified environments. Journal of Fluid Mechanics, 2002; 471: 315-337.
4. Wells MG. Two-dimensional density currents in a confined basin. Geophys. Astrophys. Fluid Dyn, 2005; 99: 199-218.
5. Arneborg L. Mixing Efficiencies in Patchy Turbulence. Journal of Physcial Oceanography, 2001; 32: 1496-1506.
6. Peters H & Johns WE. Mixing and entrainment in the Red Sea outflow plume. Part II: Turbulence characteristics. Journal of Physical Oceanography, 2005; 35: 584-600.
7. Peters, H, Bower AS & Fratantoni DM. Mixing and entrainment in the Red Sea outflow plume. Part I: Plume structure. Journal of Physical Oceanography, 2005; 35: 569-583.
8. Umlauf, L & Arneborg L. Dynamics of rotating shallow gravity currents passing through a channel. Part I: Observation of transverse structure. Journal of Physical Oceanograpgy, 2009a; 39: 2385-2401.
9. Umlauf L. & Arneborg L. Dynamics of rotating shallow gravity currents passing through a channel. Part II: Analysis. Journal of Physical Oceanograpgy, 2009b; 392: 2402-2416.
10. Baines P. Observation and Modeling of Antarctic Downslope Flows: A Review. Ocean, Ice, and Atmosphere: Interactions at the Antarctic Continental Margin Antarctic Research Series, 1998; 75: 2-49.
11. Cenedese C & Adduce C. Mixing in a density-driven current flowing down a slope in a rotating fluid. Journal of Fluid Mechanics, 2008; 604: 369-388.
12. Prandtl L. Essentials of Fluid Dynamics. Blackie, 1952.
13. Ellison TH & Turner JS. Turbulent entrainment in stratified flows. Journal of Fluid Mechanics, 1959; 6: 423-448.
14. Turner JS. Turbulent entrainment: the development of the entrainment assumption, and its application to geophysical flows. Journal of Fluid Mechanics, 1986; 173: 431-471.
15. Simpson J. The dynamics of the head of a gravity current advancing over a horizontal surface. Journal of Fluid Mechanics, 1979; 94, 477-495.
16. Simpson J. Effects of the lower boundary on the head of gravity current. Journal of Fluid Mechanics, 1972; 53: 759-768.
17. Britter RE & Linden PF. The motion of the front of a gravity current travelling down an incline. Journal of Fluid Mechanics, 1980; 99: 531-543.
18. Hallworth MA, Huppert H E, Phillips JC & Sparks SJ. Entrainment into two-dimensional and axisymmetric turbulent gravity currents. Journal of Fluid Mechanics, 1996; 308: 289-311.
19. Hacker JL, Linden PF & Dalziel SB. Mixing in lock-release gravity currents. Dyn Atmos Oceans, 1996; 24: 183-195.
20. Marino BT. The front condition for gravity currents. Journal of Fluid Mechanics, 2005; 536: 48-78.
21. Nogueira H, Adduce C, Alves E, France M. Dynamics of the head of gravity current, Environmental Fluid Mechanics, 2014; 14: 514-540.
22. Ezer T. Entrainment, diapycnal mixing and transport in three dimensional bottom gravity current simulations using the Mellor–Yamada turbulence scheme. Ocean Modelling, 2005; 9: 151-168.
23. Özgökmen TM, Iliescu T and Fisher P. Reynolds number dependence of mixing in a lock-exchange system from direct numerical and large eddy simulations. Ocean Modelling, 2009; 30: 190-206.
24. Legg S, Hallberg RW & Girton JB. Comparison of entrainment in overflows simulated by z-coordinate, isopycnal and nonhydrostatic models. Ocean Modelling, 2006; 11: 69-97.
25. Xu X, Chang YS, Peters H, Ozgokmen TM & Chassignet EP. Parameterization of gravity current entrainment for ocean circulation models using a high-order 3D nonhydrostatic spectral element model. Ocean Modelling, 2006; 14: 19-44.
26. Jackson L, Hallberg RW & Legg S. A parameterisation of shear-driven turbulence for ocean climate models. Journal of Physical Oceangraphy, 2008; 38: 1033-1053.
27. Ozgokmen TM, & Chassignet E. Dynamics of two-dimensional turbulent bottom gravity currents. Journal of Physical Oceanography, 2002; 32: 1460-1478.
28. Prastowo TR. Mixing efficiency in controlled exchange flows. Journal of Fluid Mechanics, 2008; 600: 235-244.
29. Ilıcak M. Energetics and mixing efficiency of lock-exchange flow. Ocean Modelling, 2014; 1-10.
30. Peltier WR. Mixing Efficiency in Stratified Shear Flows. Annual Review Fluid Mechanics, 2003; 35: 135-167.
31. Bhaganagar K. Direct numerical simulation of lock-exchange density currents over the rough wall in slumping phase. Journal of Hydraulic Research, 2014; 52: 386-398.
32. Morton BR, Taylor GI & Turner JS. Turbulent gravitational convection from maintained and instantaneous sources. Proceedings of Royal Society London, 1956; A234: 1-23.
33. Shin JO, Dalziel SB & Linden PF. Gravity currents produced by lock exchange. Journal of Fluid Mechanics, 2004; 521: 1.
34. Ozgokmen TM, Fischer PF, Duan J & Iliescu T. Three-Dimensional Turbulent Bottom Density Currents from a High-Order Nonhydrostatic Spectral Element Model. Journal of Physical Oceanography, 2004; 34: 2006-2026.
35. Necker FH. Mixing and dissipation in particle-driven gravity currents. Journal of Fluid Mechanics, 2005; 545: 339-372.
36. Tokyay T C. Lock-exchange gravity currents with a high volume of release propagating over a periodic array of obstacles. Journal of Fluid Mechanics, 2011; 672: 570-605.

37. Hogg CD. Inclined gravity currents filling basins: The influence of Reynolds number on entrainment into gravity currents. Physics of Fluids. 2015; 27: 096602.

38. Sher D. Gravity currents: entrainment, stratification and self-similarity. Journal of Fluid Mechanics. 2015; 784: 130-162.

39. Ottolenghi L, Adduce C, Inghilesi R, Roman F, Armenio. Mixing in lock-release gravity currents propagating up a slope. Phys. Fluids, 2016; 28.

40. Ottolenghi L, Adduce C, Inghilesi R, Armenio V, Roman F. Entrainment and mixing in unsteady gravity currents, Journal of Hydraulic ResearcH. 2016. DOI: 10.1080/00221686.2016.1174961

41. Ivey GN & Imberger J. On the nature of turbulence in a stratified fluid. Part I: The energetics of mixing. Journal of Physical Oceanography. 1990; 21: 650-658.

42. Winters KB. Available potential energy and mixing in density-stratified fluids. Journal of Fluid Mechanics, 1995; 289: 115-128.

43. Ooi SK. Numerical simulations of lock-exchange compositional gravity current. J. Fluid Mech. 2009; 635: 361-388.

44. Well M, Cenedese C & Caulfield CP. The relationship between flux coefficient and entrainment ratio in density currents. Journal of Physical Oceanography. 2010; 2713:2727.